Inorg. Chem. **2003**, *42*, 5367–5375

Design and Synthesis of a New Binucleating Ligand via Cobalt-Promoted C–N Bond Fusion Reaction. Ligand Isolation and Its Coordination to Nickel, Palladium, and Platinum

Kunal K. Kamar,[†] Srijit Das,[†] Chen-Hsiung Hung,[‡] Alfonso Castiñeiras,[§] Michael D. Kuz'min,[||] Conrado Rillo,[||] Juan Bartolomé,[||] and Sreebrata Goswami*,[†]

Department of Inorganic Chemistry, Indian Association for the Cultivation of Science, Kolkata 700 032, India, Department of Chemistry, National Changhua University of Education, Changhua, Taiwan 500, Republic of China, Departamento de Química Inorgánica, Universidade de Santiago de Compostela, Campus Universitario Sur, E-15782 Santiago de Compostela, Spain, and Instituto de Ciencia de Materiales de Aragón, CSIC—Universidad de Zaragoza, 50009 Zaragoza, Spain

Received March 24, 2003

A new polydentate bridging ligand, $NH_4C_5N{=}NC_6H_4N(H)C_5H_4N$ (HL^2), is synthesized by the cobalt-mediated phenyl ring amination of coordinated $NH_4C_5N{=}NC_6H_5$. The green cobalt complex intermediate $[Co(L^2)_2](ClO_4)$, [**1**](ClO_4), and the free ligand HL^2 were isolated and characterized. The X-ray structure of $[H_2L^2](ClO_4)$ is reported. The ligand, upon deprotonation, behaves as a bridging ligand. It reacts with $NiCl_2{\cdot}6H_2O$ and $Na_2[PdCl_4]$ to produce dimetallic complexes, $[Ni_2Cl_2(L^2)_2]$, **2**, and $[Pd_2(L^2)_2](ClO_4)_2$, [**3**]$(ClO_4)_2$, respectively. X-ray structures of these two dimetallic complexes are reported. The structure of the dinickel complex, in particular, is unique. In this complex, the two deprotonated secondary amine nitrogens of the two $[L^2]^-$ ligands bind to two nickel centers simultaneously forming a planar Ni_2N_2 arrangement. The complex [**3**]$(ClO_4)_2$ is diamagnetic while the complex **2** is paramagnetic. The results of magnetic measurements on the dinickel complex in the temperature range 1.8–300 K are reported. The system can be described as a single spin $S = 2$ in the low-temperature range $T \ll J/k$ whereas at high temperatures, $T \gg J/k$, it behaves as two independent spins $S = 1$.The reaction of $[L^2]^-$ with $K_2[PtCl_4]$, however, yielded a monometallic platinum complex, $[PtCl_3(L^2)]$, **5**, where the pyridyl nitrogen of the aminopyridyl function remained unused. The X-ray structure of the complex **4a** is reported. The bond lengths along the ligand backbones in all the complexes indicate extensive π-delocalization. Spectral data of the complexes are reported and compared.

Introduction

The ability of the 2-aminopyridine functionality to serve as a three-atom bridge has long been known.[1] This can hold metal atoms in proximity (Chart 1). Using this binding mode of 2-aminopyridine many interesting di- and polymetallic complexes have been synthesized. It is now known that this type of bridging ligand can hold the metal ions in close proximity with flexible separation, providing a suitable platform for coordination environments for intermetallic interactions.

Chart 1

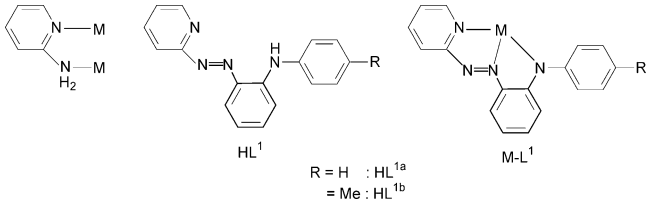

In the recent past we have been working on the coordination chemistry of a tridentate N,N,N-donor, HL^1, which has some novel features. For example, the conjugate base of HL^1 stabilizes[2,3] uncommon entities like low-spin states of man-

* Corresponding author. E-mail: icsg@mahendra.iacs.res.in. Fax: + 91 33 2473 2805.
[†] Indian Association for the Cultivation of Science.
[‡] National Changhua University of Education.
[§] Universidade de Santiago de Compostela.
[||] CSIC—Universidad de Zaragoza.

(1) (a) Chakravarty, A. R.; Cotton, F. A.; Tocher, D. A. *Organometallics* **1985**, *4*, 863. (b) Chakravarty, A. R.; Cotton, F. A.; Falvello, L. R. *Inorg. Chem.* **1986**, *25*, 214. (c) Chakravarty, A. R.; Cotton, F. A. *Inorg. Chim. Acta* **1986**, *113*, 19.

10.1021/ic034313h CCC: $25.00
Published on Web 07/22/2003

Chart 2

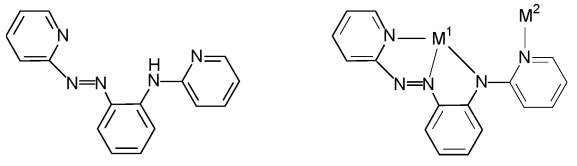

ganese(II), iron(II), and iron(III) in the complexes. A few interesting ruthenium, osmium, and rhodium complexes have also been noted[4−6] by us. The compounds of this ligand system in general display rich spectral and redox properties, which originate from strong delocalization of electronic charge along the ligand backbone. In the context of developing new materials that are suitable for efficient redox processes, such redox noninnocent ligands often play a crucial role. In its known complexes, the ligand anion $[L^1]^-$ acts as a bis-chelating ligand, which forms monometallic complexes as shown in Chart 1.

Synthesis of the ligand HL^1 was achieved[2,7] using cobalt-mediated amination reaction of coordinated 2-(phenylazo)-pyridine (pap) ligand. The above transformation is regio-selective and occurs smoothly in neat amine. With this background information, we thought it worthwhile to examine the amination reaction on coordinated pap ligand using 2-aminopyridine as the reagent. It was anticipated that fusion of the 2-aminopyridine residue to the ortho carbon of the phenyl ring of pap would produce a new ligand HL^2. This ligand is similar to HL^1 in all respects except that it has an additional pyridine N donor site for coordination. It was hoped that the additional pyridyl function of HL^2 would bind to a second metal ion. Thus a bimetallic coordination of $[L^2]^-$ may be anticipated (Chart 2).

In this paper we report the synthesis of the new bridging ligand HL^2 following amination reaction of coordinated pap ligand in a cobalt(II) complex. Its conjugate base $[L^2]^-$ indeed acts as a bridge across the two metal ions. In addition to its bridging capability, the ligand also acts as a bis-chelating tridentate N-donor, which is used to satisfy the coordination number of the metal ions. Recently we have observed[8] that this ligand forms stable complexes with d^{10}-metal ions, which absorb at unusually long wavelengths (ca. 600 nm). The coordination chemistry of the extended ligand $[L^2]^-$ involving nickel, palladium, and platinum is compared in this work.

Results and Discussion

A. Ligand Synthesis and Its Structure. The brown cationic tris-chelate, $[Co(pap)_3]^{2+}$, reacts[9] smoothly with molten 2-aminopyridine (H_2NPy) on a steam bath to produce an intense green cobalt(III) complex, $[Co(L^2)_2]^+$, $[\mathbf{1}]^+$, which was isolated as its perchlorate salt in 60% yield. Reduction of the cobalt complex by dilute hydrazine followed by removal of cobalt(II) as CoS produced the orange HL^2 in 70% yield. The synthetic reactions are shown in Scheme 1.

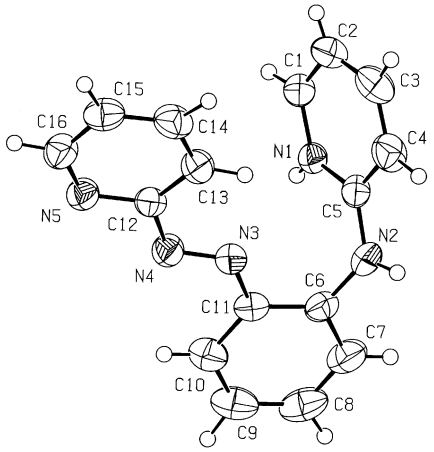

Figure 1. An ORTEP plot and atom-numbering scheme for $[H_2L^2]^+$ in $[H_2L^2](ClO_4)$.

Scheme 1

$$[Co(pap)_3]^{2+} \xrightarrow[\text{brown}]{H_2N\text{-}Py} [Co(L^2)_2]^+ \xrightarrow[\text{green}]{N_2H_4} [Co(L^2)_2] \xrightarrow[\text{brown}]{(NH_4)_2S_x} CoS + HL^2 \quad (\text{orange})$$

The green diamagnetic cobalt(III) compound is a 1:1 electrolyte in acetonitrile and shows a highly resolved ^1H NMR spectrum. All twelve resonances in its spectrum were visible (Supporting Information, Figure S1). Notably each kind of proton in the complex, $[\mathbf{1}]^+$, of the anionic ligand $[L^2]^-$ gave rise to one signal. Thus the two ligands in it are magnetically equivalent, indicating the presence of a 2-fold symmetry axis. Its analytical data are in complete agreement with its formulation. Selected spectral data are collected in Table 1. These are similar[8] to those of the analogous $[Co(L^1)_2]^+$ complex. The orange ligand HL^2 was obtained as a crystalline solid which melts at 90 °C. Its FAB mass spectrum showed an intense peak at m/z 276 confirming its formulation. The ligand dissociates the amine proton easily ($pK_a = 8.6 \pm 0.1$). Its acidity is comparable[2] to that of HL^1. The ligand HL^2, though crystalline, did not produce X-ray quality crystals. However, the perchlorate salt of its conjugate acid, $[H_2L^2]^+$, formed good crystals for its X-ray structure determination. Figure 1 shows the ORTEP plot of $[H_2L^2]^+$, and its bond parameters are collected in Table 2. This indeed confirms the formation of HL^2 from the cobalt-promoted C−N fusion reaction as shown in Scheme 1. In this compound only one of the two pyridyl nitrogens, viz., the aminopyridyl function, is protonated. The N−N distance in it is 1.246(3) Å, confirming[10] its double-bond character. The rest of the bond lengths are normal.

B. Dinickel Complex. We recently have reported[3] the synthesis and properties of the monometallic $[Ni(L^1)_2]$

(2) Saha, A.; Majumdar, P.; Goswami, S. *J. Chem. Soc., Dalton Trans.* **2000**, 1703.
(3) Saha, A.; Majumdar, P.; Peng, S.-M.; Goswami, S. *Eur. J. Inorg. Chem.* **2000**, 2631.
(4) Das, C.; Ghosh, A. K.; Hung, C.-H.; Lee, G.-H.; Peng, S.-M.; Goswami, S. *Inorg. Chem.* **2002**, *41*, 7125.
(5) Das, C.; Peng, S.-M.; Lee, G.-H.; Goswami, S. *New J. Chem.* **2002**, *26*, 222.
(6) Das, C.; Saha. A.; Hung, C.-H.; Lee, G.-H.; Peng, S.-M.; Goswami, S. *Inorg. Chem.* **2003**, *42*, 198.
(7) Saha, A.; Ghosh, A. K.; Majumdar, P.; Mitra, K. N.; Mondal, S.; Rajak, K. K.; Falvello, L. R.; Goswami, S. *Organometallics* **1999**, *18*, 3772.
(8) Das, S.; Hung, C.-H.; Goswami, S. *Inorg. Chem.*, in press.
(9) Mahapatra, A. K. Ph.D. Thesis, Jadavpur University, Calcutta, India, 1986.
(10) Saha, A.; Das, C.; Peng, S.-M.; Goswami, S. *Indian J. Chem., Sect. A* **2001**, *40A*, 198.

Table 1. Optical Spectral Data

compound	λ_{max}/nm (ϵ/ M^{-1} cm^{-1})[a]	IR (ν, cm^{-1})[c]		
		ν(C=N)	ν(N=N)	$\nu(ClO_4)^-$
[**1**](ClO_4)	860 (8535), 775 (11665), 705 (10965), 655 (8285), 400 (18865), 290[b] (29580), 240 (49530)	1585	1370	1075, 610
HL^2	450 (5330), 312 (14550), 275 (19025)	1595	1450	
2	590 (9855), 350 (25610), 280 (36540), 250 (35930)	1605	1385	
[**3**](ClO_4)$_2$	905 (7055), 825 (8060), 430[b] (9235), 330 (28220), 230 (43925)	1599	1384	1087, 627
4a	1065 (3030), 930 (6090), 835 (6105), 740 (3825), 460[b] (4420), 380[b] (10260), 350 (17795), 235 (27785)	1606	1377	
4b	1060 (2420), 930 (4630), 840 (4700), 745 (3040), 455[b] (3950), 380[b] (8205), 350 (14040), 235 (22220)	1602	1384	
5	1170 (2015), 1020 (3585), 900 (3135), 810 (1900), 470[b] (7510), 355 (16875), 280 (19985)	1599	1380	
6a	1240 (1430), 1055 (2815), 895 (3425), 795 (3550), 715 (2615), 655 (1505), 470[b] (6710), 355 (13960), 275 (27540)	1600	1385	
6b	1245 (1440), 1060 (2735), 915 (3230), 800 (3255), 725 (2445), 660 (1460), 475[b] (6275), 355 (13375), 265 (19545)	1597	1384	

[a] Solvent, acetonitrile for the compounds [**1**](ClO_4), HL^2, **2**, [**3**](ClO_4), and **4** and dimethylformamide for the compounds **5** and **6**. [b] Shoulder. [c] In KBr disk.

Table 2. Selected Bond Lengths (Å) and Bond Angles (deg) of [H_2L^2](ClO_4), **2**·H_2O, [**3**](ClO_4)$_2$·H_2O, **4a**, and **5**

$[H_2L^2](ClO_4)$

N(1)−C(5)	1.335(4)	C(6)−C(11)	1.400(4)	N(4)−C(12)	1.427(4)
N(2)−C(5)	1.350(4)	N(3)−C(11)	1.413(4)	N(5)−C(12)	1.336(4)
N(2)−C(6)	1.406(4)	N(3)−N(4)	1.246(3)		

$[Ni_2Cl_2(L^2)_2]$·H_2O, **2**·H_2O

Ni(1)−N(14)	2.094(3)	Ni(1)−N(11)	2.099(4)	N(12)−N(13)	1.271(5)
Ni(1)−N(34)	2.277(3)	Ni(1)−N(13)	1.996(3)	N(13)−C(16)	1.404(6)
Ni(2)−N(14)	2.277(3)	Ni(1)−Cl(1)	2.3482(12)	N(14)−C(21)	1.379(5)
Ni(2)−N(34)	2.103(3)	N(11)−C(15)	1.347(5)	N(14)−C(22)	1.392(5)
Ni(1)−N(35)	2.056(3)	N(12)−C(15)	1.423(6)	N(15)−C(22)	1.343(5)
Ni(1)−N(14)−Ni(2)	93.32(12)	Ni(1)−N(34)−Ni(2)	93.09(12)		

$[Pd_2(L^2)_2](ClO_4)_2$·H_2O, [**3**](ClO_4)$_2$·H_2O

Pd(1)−N(1)	1.992(7)	C(6)−C(11)	1.427(10)	N(7)−C(21)	1.410(9)
Pd(1)−N(3)	1.916(6)	N(4)−C(11)	1.343(9)	N(7)−N(8)	1.288(8)
Pd(1)−N(4)	1.967(6)	N(4)−C(12)	1.370(10)	N(8)−C(22)	1.396(9)
Pd(1)−N(10)	2.012(7)	Pd(2)−N(6)	2.024(7)	C(22)−C(27)	1.435(11)
N(1)−C(5)	1.363(10)	Pd(2)−N(8)	1.919(7)	N(9)−C(27)	1.344(10)
N(2)−C(5)	1.390(9)	Pd(2)−N(9)	1.999(7)	N(9)−C(28)	1.366(11)
N(2)−N(3)	1.277(7)	Pd(2)−N(5)	2.044(7)		
N(3)−C(6)	1.379(8)	N(6)−C(21)	1.364(10)		
N(1)−Pd(1)−N(3)	78.6(3)	N(3)−Pd(1)−N(4)	81.6(2)		
N(8)−Pd(2)−N(9)	82.9(4)	N(6)−Pd(2)−N(8)	78.8(3)		

$[PdCl(L^{1a})]$, **4a**

Pd(1)−N(1)	2.029(3)	N(1)−C(11)	1.338(4)	N(2)−N(3)	1.305(3)
Pd(1)−N(2)	1.930(3)	C(6)−C(11)	1.440(4)	N(3)−C(5)	1.388(4)
Pd(1)−N(4)	2.029(3)	N(2)−C(6)	1.360(4)	N(4)−C(5)	1.369(4)
Pd(1)−Cl(1)	2.3031(11)				
N(1)−Pd(1)−N(2)	81.83(13)	N(2)−Pd(1)−N(4)	79.00(13)		

$[PtCl_3(L^2)]$, **5**

Pt(1)−N(1)	2.050(4)	Pt(1)−Cl(3)	2.3159(12)	C(6)−C(11)	1.430(6)
Pt(1)−N(3)	1.967(4)	N(1)−C(5)	1.376(5)	N(4)−C(11)	1.342(6)
Pt(1)−N(4)	2.041(4)	N(2)−C(5)	1.408(5)	N(4)−C(12)	1.416(5)
Pt(1)−Cl(1)	2.3196(12)	N(2)−N(3)	1.272(5)	N(5)−C(12)	1.342(6)
Pt(1)−Cl(2)	2.3309(12)	N(3)−C(6)	1.360(5)		
N(1)−Pt(1)−N(3)	79.32(14)	N(3)−Pt(1)−N(4)	82.05(14)		

complex, which is green in color. The ligand $[L^1]^-$, in the nickel complex, acts as a monoanionic bis-chelating tridentate donor, two of which satisfy the six coordination number of the central Ni(II) ion. In contrast, the reaction of hydrated salt $NiCl_2$·$6H_2O$ with $[L^2]^-$ in equimolar proportions produced an intense and bright blue solution. The usual workup followed by crystallization of the crude mass produced a molecular dinickel complex, $[Ni_2Cl_2(L^2)_2]$, **2**, in an excellent yield (80%). This showed all characteristic IR stretches for the coordinated ligands. The dinickel complex is soluble in all common solvents. Its UV−vis spectrum consists of several charge-transfer transitions, of which the broad band near 600 nm is responsible for its blue color.

The dinickel complex forms dark blue crystals, whose single-crystal X-ray structure has been solved. A labeled ORTEP plot of the complex **2** is shown in Figure 2, and

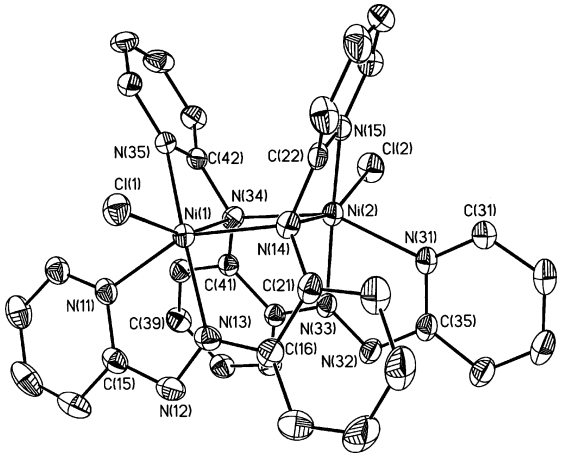

Figure 2. An ORTEP plot and atom-numbering scheme for the molecular complex $[Ni_2Cl_2(L^2)_2]$, **2**. Hydrogen atoms are omitted for clarity.

selected bond parameters are collected in Table 2. Two nickel ions in this molecule are in a highly distorted octahedral geometry with each nickel surrounded by a N_5Cl environment. The two extended ligands satisfy five coordination sites of each nickel ion and act as bridges across the two nickel centers. The coordination mode of the anionic $[L^2]^-$ ligand in this molecule is unique in many respects. In addition to the pyridyl nitrogens, viz., N(15) and N(35) of the amino-pyridyl function, the two deprotonated amine nitrogens, viz., N(14) and N(34), bind simultaneously to two nickel ions. Double-bridged dinuclear complexes with bridging coordination of a deprotonated secondary amine function and having a $M_2(\mu\text{-}NR_2)_2$ core are scarce[11] in the literature. The two amide nitrogens together with two nickel(II) ions in this complex form a plane with no atom deviating by more than 0.033 Å. For this, the 2-pyridylamide functions, $[N\text{-}Py]^-$, of each $[L^2]^-$ form highly strained four-member chelate rings comprising Ni(1), N(34), C(42), N(35) and Ni(2), N(14), C(22), N(15). Four-member chelates for dithiocarbamates are common, and those for carboxylates and nitrates are also known; however, such strained coordination is not common for an extended multidentate ligand. Of the five Ni−N bonds around each nickel ion, the two Ni−N(azo) lengths [e.g., Ni(1)−N(13), 1.996(3) Å] are appreciably short compared to the other Ni−N bonds. This may[12,13] be due to the presence of extensive charge delocalization along the ligand backbone of the anionic ligand $[L^2]^-$. Consequently, the −N═N− lengths are elongated and the azo nitrogen to phenyl carbon distances as well as the lengths of deprotonated amide nitrogen bond to the phenyl group of pap are shorter than a C−N single bond. A similar effect was noted before[3] in the structure of the monometallic complex, $[Ni(L^1)_2]$. We also note that the Ni−N(amide) lengths in the Ni_2N_2 ring are of two types; the Ni(1)−N(14) and Ni(2)−N(34) [av 2.099(3) Å] are smaller than the other two Ni−N bonds [av 2.277(3) Å], indicating that the bridging amide nitrogens do not interact equally with the two nickel ions. The separation between the two nickel ions in this molecule is 3.1818(8) Å, which does not suggest[11b] any Ni−Ni bonding.

Magnetic susceptibility of the dinickel complex was measured at temperatures ranging from 1.8 to 300 K and is presented in Figure 3 as $(3k\chi T/N\mu_B^2)^{1/2}$ vs T, where χ is the molar susceptibility, N is Avogadro's number, and μ_B is Bohr's magneton. Clearly, the quantity plotted in Figure 3 is not a constant, as it would be in a simple paramagnet. The magnetic behavior of the nickel dimer can be understood as that of an exchange-coupled pair of spins $S = 1$. The following Hamiltonian describes the system:

$$\hat{H} = -2J\hat{\mathbf{S}}_1\cdot\hat{\mathbf{S}}_2 - D(\hat{S}_{1z}^2 + \hat{S}_{2z}^2) + g\mu_B\mathbf{H}\cdot\hat{\mathbf{S}}$$

which includes Heisenberg exchange, zero-field splitting, and interaction with the magnetic field. The exchange integral, J, is positive, which corresponds to ferromagnetic interaction. In the low-temperature range, $T \ll J/k$, the system can be described as a single spin $S = 2$, whereas at high temperatures, $T \gg J/k$, it behaves as two independent spins $S = 1$. Finally, at very low temperatures the effect of zero-field splitting becomes apparent as the data points plotted in Figure 3 drop sharply below $T \sim 10$ K.

For better stability, the determination of the adjustable parameters was carried out in two stages: (i) At temperatures to the right of the maximum ($T > 20$ K), where the zero-field splitting is irrelevant, the data were fitted to a simplified formula, which neglected D but included a temperature-independent Van Vleck term, $N\alpha$. The best-fit values are $J = 18.5$ cm^{-1}, $g = 2.14$, $\alpha = 1.7 \times 10^{-27}$ cm^3. (ii) Using the formalism[14,15] of Ginsberg et al., which allows for a nonzero D, the entire data set was fitted. At this stage D was the sole adjustable parameter, while J, g, and α were kept fixed at the values established previously. In this way $D = -9$ cm^{-1} was found. The final calculated curve is shown in Figure 3. However, the most convincing confirmation of the adopted interpretation of the magnetic susceptibility data comes from low-temperature magnetization curves, which are submitted as Supporting Information.

(11) (a) Aullón, G.; Lledós, A.; Alvarez, S. *Inorg. Chem.* **2000**, *39*, 906. (b) Holland, P. L.; Andersen, R. A.; Bergman, R. G. *J. Am. Chem. Soc.* **1996**, *118*, 1092. (c) Hope, H.; Olmstead, M. M.; Murray, B. D.; Power, P. P. *J. Am. Chem. Soc.* **1985**, *107*, 712.

(12) This may also happen due to geometric reason. For a bis-chelating bidentate ligand, forming two five-member chelate rings, the M−N bond length for the middle nitrogen is smaller[13] than those for the terminal nitrogens.

(13) (a) Pramanik, N. C.; Pramanik, K.; Ghosh, P.; Bhattacharya, S. *Polyhedron* **1998**, *17*, 1525. (b) Matsumoto, N.; Motoda, Y.; Matsuo, T.; Nakashima, T.; Re, N.; Dahan, F.; Tuchagues, J.-P. *Inorg. Chem.* **1999**, *38*, 1165. (c) Bruin, B. De.; Bill, E.; Bothe, E.; Weyhermuller, T.; Wieghardt, K. *Inorg. Chem.* **2000**, *39*, 2936.

(14) Ginsberg, A. P.; Martin, R. L.; Brookes, R. W.; Sherwood, R. C. *Inorg. Chem.* **1972**, *11*, 2884.

(15) Neglect of the interdimer exchange interaction in the above approach is justified by the weakness of that interaction. Thus, between 1.8 and 5 K, the susceptibility follows the Curie−Weiss law, $\chi = C/(T - \theta)$, with $C = 4.2$ K emu/mol and $\theta \approx -2$ K. The interdimer exchange integral is then estimated as $zJ' = \theta/4 \approx -0.5$ K, z being the number of nearest neighbors. On the other hand, $D < 0$, hence the ground state of the dimer is a nonmagnetic singlet, therefore the presence of the small interdimer interaction, $z|J'| \ll |D|$, is irrelevant. Any possibility of a positive zero-field splitting can be ruled out, since this would have meant a doublet ground state and a Curie−Weiss behavior with a much smaller Curie constant, $C = 2.3$ K emu/mol. This conclusion holds regardless of the interdimer interaction, which affects θ but not C.

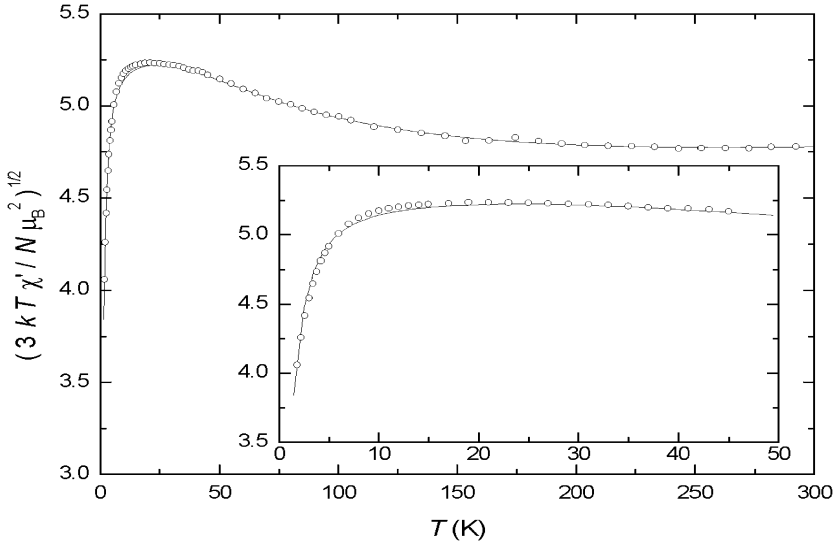

Figure 3. A plot of $(3k\chi T/N\mu_B^2)^{1/2}$ vs T (K) for $[Ni_2Cl_2(L^2)_2]\cdot H_2O$, **2**·$H_2O$. The line represents the best fit, and the points are experimental data.

Previous studies on the Ni dimers containing Ni_2O_2 were reported, where the exchange coupling constant was shown[16] to be directly proportional to the Ni−O−Ni bridge angles or Ni−Ni separation. The bridge bond angle Ni−N−Ni in our system is ca. 93°, and the two-nickel centers are coupled ferromagnetically. As far as we are aware no other experimental result on the system containing a Ni_2N_2 core was available. The magnetostructural data available for a few halo-bridged nickel(II) complexes[17] are indicative of ferromagnetic coupling taking place via 90° Ni−X−Ni (X = Cl, Br) interactions. More results are accessible for azido-bridged nickel(II) complexes. Compounds with end-on bridges are known to exhibit ferromagnetic exchange while end-to-end bridge systems give rise to antiferromagnetic interaction.[18,19] For several end-on μ_2-N_3 nickel(II) complexes the reported J values lie between 20 and 49 cm^{-1}.

C. Palladium Complexes. A dipalladium complex having the composition $[Pd_2(L^2)_2](ClO_4)_2$, $[\mathbf{3}](ClO_4)_2$, was obtained in 70% yield from the reaction of deprotonated HL^2 and $Na_2[PdCl_4]$ in equimolar proportions in methanol at room temperature. Dilute NEt_3 was used for the deprotonation of HL^2. The cationic palladium complex $[\mathbf{3}]^{2+}$ was isolated as its perchlorate salt. It gave consistent analysis confirming its formulation. In solution, the complex behaves as a 1:2 electrolyte (Λ_M = 240 Ω^{-1} cm^2 mol^{-1} in 1 × 10^{-3} M acetonitrile). The diamagnetic complex $[\mathbf{3}]^{2+}$ shows the resolved ^1H NMR spectrum (Figure 4). The spectrum is in agreement with the crystal structure of $[Pd_2(L^2)_2](ClO_4)_2\cdot H_2O$ (vide infra). Notably, each kind of proton of the coordinated anioinc ligand $[L^2]^-$ gave rise to one signal. Thus the two ligands in $[\mathbf{3}]^{2+}$ are magnetically equivalent, indicating the presence of a 2-fold symmetry axis. Notably, the −NH resonance in $[\mathbf{3}]^{2+}$ was absent.

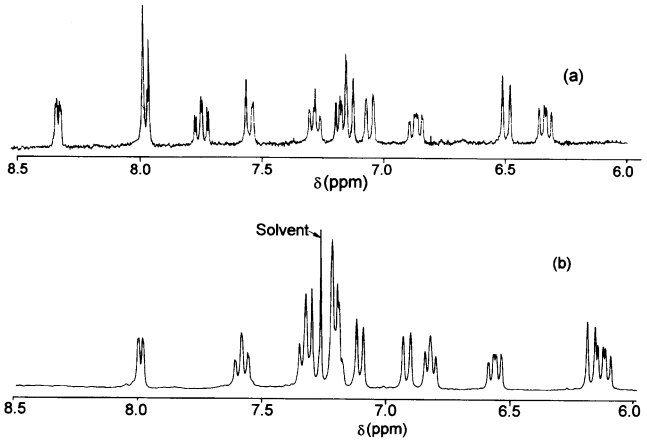

Figure 4. ^1H NMR spectra of (a) $[Pd_2(L^2)_2](ClO_4)_2$, $[\mathbf{3}](ClO_4)_2$, in DMSO-d_6, and (b) $[PdCl(L^{1a})]$, **4a**, in $CDCl_3$.

The structural analysis of $[\mathbf{3}](ClO_4)_2$ has indeed authenticated the dimetallic coordination of $[L^2]^-$. The 2-(phenylazo)pyridyl part [N(1) and N(3)] along with the deprotonated amine nitrogen [N(4)] bind to a palladium center, Pd(1) as a tridentate donor. The pyridyl nitrogen [N(5)] of this cannot bind to the same metal; instead it coordinates to a second palladium center [Pd(2)]. The second $[L^2]^-$ ligand binds in a similar fashion, as a tridentate donor around Pd(2), and binds to Pd(1) through its pyridyl [N(10)] nitrogen. The two ligands thus satisfy four coordination of each palladium. The complex as a whole is a dication, and there are two perchlorate counterions along with two water molecules with 0.5 occupancy on each oxygen atom as crystallization in the asymmetric unit. Figure 5 shows the ORTEP plot and atom-numbering scheme for the cationic complex $[Pd_2(L^2)_2]^{2+}$. Thus the bridging coordination mode of the ligand $[L^2]^-$ in its palladium complex is as anticipated. However, the bridging coordination mode of the $[NAr_2]^-$ function was not observable in the case of the dipalladium system. This is in

(16) Nanda, K. K.; Thompson, L. K.; Bridson, J. N.; Nag, K. *J. Chem. Soc., Chem. Commun.* **1994**, 1337.
(17) (a) Laskowski, E. J.; Felthouse, T. R.; Hendrickson, D. N.; Long, G. *Inorg. Chem.* **1976**, *15*, 2908. (b) Journaux, Y.; Kahan, O. *J. Chem. Soc., Dalton Trans.* **1979**, 1575.
(18) (a) Ribas, J.; Monfort, M.; Diaz, C.; Bastos, C.; Solans, X. *Inorg. Chem.* **1993**, *32*, 3557. (b) Karmakar T. K.; Chandra, S. K.; Ribas, J.; Mostafa, G.; Lu, T. H.; Ghosh, B. K. *Chem. Commun.* **2002**, 2364. (c) Ribas, J.; Monfort, M.; Ghosh, B. K.; Solans, X. *Angew. Chem., Int. Ed. Engl.* **1994**, *33*, 2087 and references therein.
(19) Mohanta, S.; Nanda, K. K.; Werner, R.; Haase, W.; Mukherjee, A. K.; Dutta, S. K.; Nag, K. *Inorg. Chem.* **1997**, *36*, 4656 and references therein.

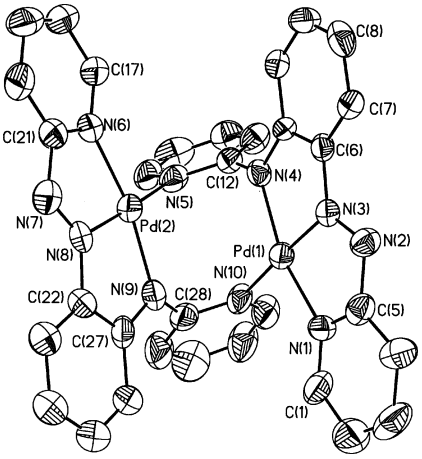

Figure 5. An ORTEP plot and atom-numbering scheme for $[Pd_2(L^2)_2]^{2+}$ in $[Pd_2(L^2)_2](ClO_4)_2$, $[\mathbf{3}](ClO_4)_2$. Hydrogen atoms are omitted for clarity.

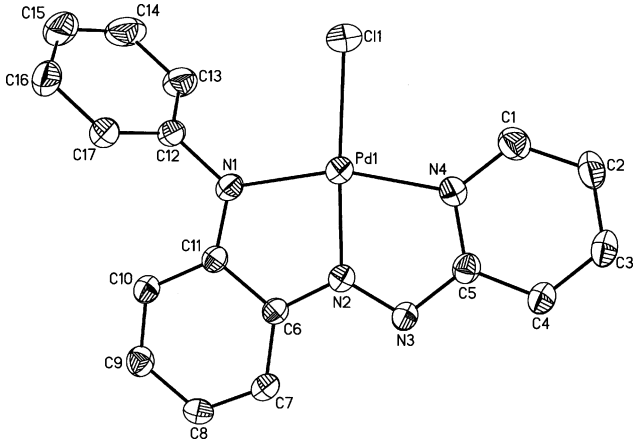

Figure 6. An ORTEP plot and atom-numbering scheme for the molecular complex $[PdCl(L^{1a})]$, **4a**. Hydrogen atoms are omitted for clarity.

contrast to the observation noted before in the dinickel complex. Selected bond distances of the above dipalladium complex are collected in Table 2. The two azo nitrogens of the anionic tridentate ligands approach the metal center closest with Pd(1)−N(3), 1.916(6) Å, and Pd(2)−N(8), 1.919(7) Å, respectively. Indications of significant backbone conjugation in each of the coordinated anionic ligands were noted. Thus the average of the two N−C lengths, viz., N(4)−C(11) and N(9)−C(27), 1.343(9) Å, is considerably shorter than a N−C single bond length. The average of N−N distances of the azo nitrogen also indicates elongation, which is consistent with the delocalization along the ligand backbone of the anionic ligand $[L^2]^-$.

We then thought it worthwhile to scrutinize a similar reaction of $Na_2[PdCl_4]$ with $[L^1]^-$ under an identical condition for a comparison. We wish to reiterate here that a phenyl group in $[L^1]^-$ replaces a 2-pyridyl group of $[L^2]^-$. In line with our strategy $Na_2[PdCl_4]$ was reacted with HL^1 in methanol in the presence of NEt_3 as a base. A brown molecular compound of composition $[PdCl(L^1)]$, **4**, was isolated in almost quantitative yield. This gave a resolved ^1H NMR spectrum (Figure 4). The X-ray structure of a representative $[PdCl(L^{1a})]$, **4a**, was determined. The ORTEP plot and atom-numbering scheme for **4a** are shown in Figure 6. The compound **4a** is monometallic. The coordination sphere involves PdN_3Cl. The tridentate ligand $[L^1]^-$ along with one chloride completes a distorted square planar geometry. The bond lengths in this molecule indicate significant conjugation along the ligand backbone. The Pd(1)−N(2) is shortest [1.930(3) Å] and is comparable to those [Pd(1)−N(3) and Pd(2)−N(8)] observed in the dipalladium complex, $[\mathbf{3}]^{2+}$.

The solution colors of the palladium compounds are brown. Selected spectral characterization data are collected in Table 1. Multiple and overlapping absorption of moderate intensities was observed in the near-infrared region. Interestingly, the intensities of transitions for the dipalladium complex, $[\mathbf{3}](ClO_4)_2$, are much higher than those for the monometallic complex, **4**. Interligand charge-transfer transitions were noted for both the complexes in the UV region. Semiempirical EHMO calculations[20] on these indicate that while the HOMOs are the admixture of metal and ligand orbitals, the LUMOs are predominantly ligand orbitals. Hence the low-energy transitions may best be ascribed as $\pi-\pi^*$ transitions.

D. Platinum Complexes. Unlike its palladium congener, the product of reaction of the platinum salt, $K_2[PtCl_4]$, and either of the ligands HL^1 and HL^2 was not as anticipated. The above reactions do not proceed at all in methanol. On prolonged stirring (>2 h) some insoluble precipitate appeared presumably due to formation of platinum metal. However, reaction of $K_2[PtCl_4]$ with the deprotonated ligand, $[L^2]^-$, was observed to occur in boiling acetonitrile in the presence of air. The reaction mixture became green in about 2 h. The usual workup followed by crystallization of the above reaction mixture produced a crystalline molecular complex of formula $[PtCl_3(L^2)]$, **5**. In this compound the ligand $[L^2]^-$ coordinates as a tridentate ligand using one pyridyl, azo, and deprotonated amine nitrogens. The second pyridyl nitrogen of amino pyridyl function remained unused (vide infra). Notably, the metal ion, during this reaction, undergoes two-step oxidation [Pt(II) → Pt(IV)], which is brought about by air. A similar Pt(IV) product was isolated from the reaction of $K_2[PtCl_4]$ and HL^1. Thus the results, in the case of platinum, are different from that observed in the two former cases. Differences in redox properties of the reference metal ions are no doubt responsible for this. Platinum(II) being more susceptible to redox processes undergoes reduction to platinum metal in a reducing solvent like methanol. It, on the otherhand, undergoes oxidation to platinum(IV) by air in acetonitrile. In its reaction with $[L^2]^-$ the dimetallic complex was not observed due to inertness of the resultant platinum(IV) complex, $[PtCl_3(L^2)]$, **5**, toward substitution. In contrast, the corresponding palladium(II) complex, the plausible intermediate, is labile and undergoes dimerization easily to produce a dimetallic complex. The two types of reactions of palladium and platinum are compared in Scheme 2. It may relevant to note here that the above platinum(IV) complex is extremely inert and is unreactive to Ag(I) even in boiling acetonitrile.

(20) Mealli, C.; Proserpio, D. M. *J. Chem. Educ.* **1990**, *67*, 399.

Scheme 2

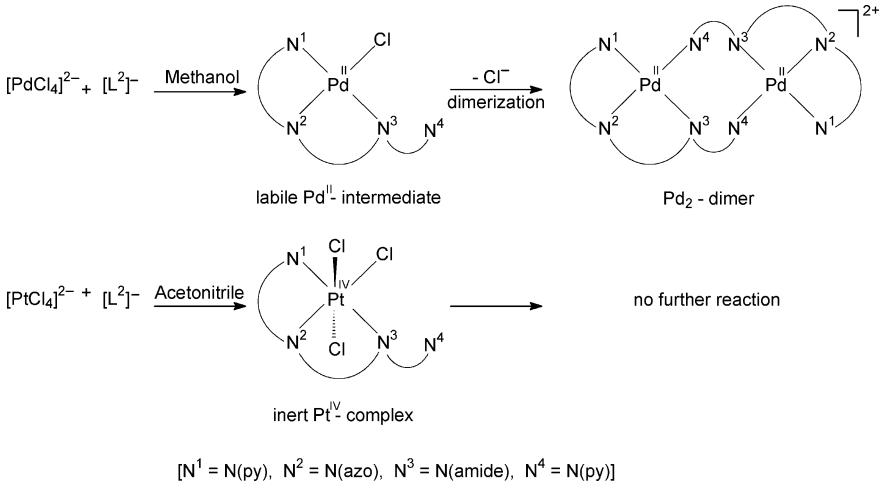

The platinum(IV) complex, $[PtCl_3(L^2)]$, **5**, formed suitable X-ray quality crystals. A view of the molecular complex is shown in Figure 7. In this complex, the platinum center is surrounded by a distorted octahedral coordination environment by three chloride ligands and the tridentate monoanionic bis-chelating ligand. One of the two pyridyl nitrogens [N(5)] remained uncoordinated. The selected bond parameters are collected in Table 2. Taken together, the lengthening of the azo −N═N− length in $[L^2]^-$ and the shortening of the N−C distances alongside of the azo moiety, with respect to the corresponding distances in $[H_2L^2]^+$ (Table 2), indicate considerable delocalization of π-electron density in $[L^2]^-$. The central Pt−N bond of the anionic ligand, Pt(1)−N(3), 1.967(4) Å, is significantly shorter than the other two similar Pt−N distances with average 2.045(4) Å.

The ^{1}H NMR spectra of the two platinum(IV) complexes are similar in nature, but they are different from those observed for the corresponding palladium(II) complexes. The combination of several high-intensity visible range transitions in their solution spectra characterizes these platinum complexes. In addition, ligand-based transitions were observed in the UV region. Semiempirical EHMO calculations[20] using the X-ray structural parameters of $[PtCl_3(L^2)]$, **5**, indicate that the HOMO is a mixed metal−ligand orbital while the acceptor orbital LUMO is a combination of ligand orbitals with only small contributions of the metal orbitals. Notably, the lowest energy transitions in platinum(IV) complexes are red shifted considerably compared to the corresponding palladium(II) complexes.

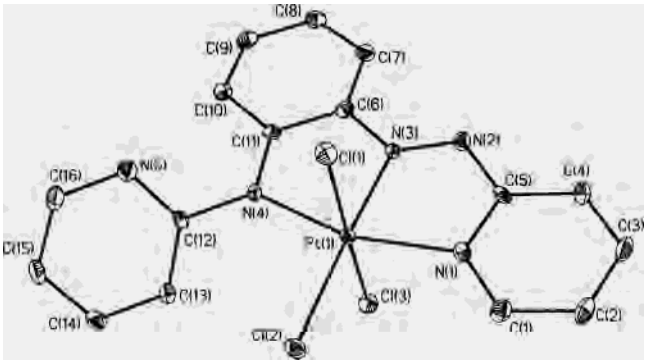

Figure 7. An ORTEP plot and atom-numbering scheme for the molecular complex $[PtCl_3(L^2)]$, **5**. Hydrogen atoms are omitted for clarity.

Conclusion

The successful design and synthesis of a new N-donor bridging ligand, [2-(2-pyridylamino)phenylazo]pyridine have been achieved by cobalt-mediated fusion of 2-aminopyridine on coordinated 2-(phenylazo)pyridine. This acts as a potential bridging ligand. Two dimetallic complexes of nickel and palladium have been synthesized. The coordination mode of the anionic ligand in the dinickel complex is unique and different from that in the case of the dipalladium complex. In the former example, the pyridyl and the deprotonated secondary amine nitrogens act as bridge across the two nickel centers. It may be relevant to note that such a bridging mode of a $[NR_2]^-$ function is not available in the literature. The two nickel centers in the dinickel complex are ferromagnetically coupled with $J = 18.5$ cm^{-1}. A different type of reaction was, however, observed in the case of platinum. Platinum(II), being redox active, undergoes two-step oxidation to result in a platinum(IV) monometallic complex of $[L^2]^-$ in air. This monometallic Pt(IV) complex is absolutely inert toward substitution and cannot dimmerize to produce a dimetallic complex.

Experimental Section

Materials. The starting complex $[Co(pap)_3](ClO_4)_2$ and the HL^1 were prepared[2] by a reported procedure. The salts $PdCl_2$ and $K_2[PtCl_4]$ were obtained form Arora-Matthey, Kolkata. $PdCl_2$ was converted to $Na_2[PdCl_4]$ as before.[21] Solvents and chemicals used for synthesis were of analytical grade. **CAUTION:** Perchlorate salts of metal complexes can be explosive. Although no detonation tendencies have been observed, care is advised and handling of only small quantities recommended.

Physical Measurements. A JASCO V-570 spectrophotometer was used to record the electronic spectra. The IR spectra were recorded with a Perkin- Elmer 783 spectrophotometer. ^{1}H NMR spectra were measured in $CDCl_3$ and DMSO-d_6 with a Brucker

(21) (a) Chattopadhyay, P.; Nayak, M. K.; Bhattacharya, S. P.; Sinha, C. *Polyhedron* **1997**, *16*, 1291. (b) Basuli, F.; Chattopadhyay, P.; Sinha, C. *Polyhedron* **1996**, *15*, 2439.

Avance DPX 300 spectrometer, and $SiMe_4$ was used as the internal standard. A Perkin-Elmer 240C element analyzer was used to collect microanalytical data (C, H, N). Electrical conductivity was measured by using a Systronics direct reading conductometer 304. Melting points were determined with the help of a capillary fitting Mel. Temp. II (Laboratory Devices Inc., USA) apparatus.

Magnetic measurements were performed in a commercial SQUID magnetometer from Quantum Design. First, the ac magnetic moment was measured as a function of temperature between 1.8 and 300 K. The applied ac field had an amplitude of 4.5 Oe at 10 Hz. From the measured ac magnetic moment, the in-phase magnetic susceptibility, χ', and the out-of phase magnetic susceptibility, χ'', were calculated. At first glance $\chi'(T)$ was paramagnetic in the whole temperature range, but not a simple paramagnet following a unique Curie law $\chi'(T) = C/T$. Confirming the paramagnetic behavior, χ'' was negligible in the whole temperature range. For a more complete magnetic study, isothermal magnetization curves $M(\mu_0 H)$ were taken at $T = 1.8$ and 5 K, in the magnetic field range $0 < \mu_0 H < 5$ *T*.

Synthesis of Complexes. $[Co(L^2)_2](ClO_4)$, [1](ClO_4). A mixture of $[Co(pap)_3](ClO_4)_2$ (0.2 g, 0.25 mmol) and 2-aminopyridine (0.1 g, 1.06 mmol) was heated on a steam bath for 1 h. The initial brown color gradually changed to intense green. The cooled green mixture was thoroughly washed with diethyl ether. Crystallization of the crude green product from a dichloromethane−hexane mixture yielded crystalline $[Co(L^2)_2](ClO_4)$ in 60% yield.

Anal. Calcd for $C_{32}H_{26}N_{10}ClO_5Co$: C, 53.01; H, 3.58; N, 19.32. Found: C, 53.06; H, 3.53; N, 19.25.

Isolation of [2-(2-Pyridylamino)phenyl]azopyridine (HL^2) from the Complex [1](ClO_4). The cobalt complex $[Co(L^2)_2](ClO_4)$ (0.15 g, 0.21 mmol) was dissolved in ethanol (30 mL), and to it were added hydrazine hydrate (5 mL) and yellow ammonium sulfide (5 mL). The mixture was then stirred for 30 min at room temperature. The resulting orange-yellow solution was evaporated under vacuum, then extracted with dichloromethane, and subjected to a silica gel PTLC technique. An orange-yellow band was eluted with a toluene−chloroform mixture (1:2), which on evaporation yielded orange crystals of HL^2 in 70% yield. FAB mass (M): 276. Mp: 90 °C. $pK_a = 8.6 \pm 0.1$. Anal. Calcd for $C_{16}H_{15}N_5O$: C, 65.53; H, 5.12; N, 23.89. Found: C, 65.55; H, 5.15; N, 23.92.

$[Ni_2Cl_2(L^2)_2]$, 2. The ligand HL^2 (0.1 g, 0.36 mmol) was dissolved in methanol (30 mL), and to it were added 1−2 drops of dilute triethylamine. To the deprotonated ligand solution was added a methanolic solution of $NiCl_2 \cdot 6H_2O$ (0.086 g, 0.362 mmol) with constant stirring. The mixture was stirred for 1 h at room temperature. The color of the solution changed to bright blue. The resultant mixture was filtered, and the solvent was evaporated under vacuum. Crystalline $[Ni_2Cl_2(L^2)_2]$ was finally obtained by slow diffusion of a dichloromethane solution of the compound into hexane. Yield: 80%. Anal. Calcd for $C_{32}H_{26}N_{10}Cl_2ONi_2$: C, 50.86; H, 3.44; N, 18.54. Found: C, 50.82; H, 3.46; N, 18.50.

$[Pd_2(L^2)_2](ClO_4)_2$, [3]$(ClO_4)_2$. The ligand HL^2 (0.1 g, 0.36 mmol) was dissolved in methanol (30 mL), and to it were added 1−2 drops of dilute triethylamine. To the deprotonated ligand solution was added a methanolic solution of $Na_2[PdCl_4]$ (0.11 g, 0.37 mmol), and the mixture was stirred for 30 min at room temperature. The color of the mixture gradually became greenish brown. The compound was precipitated from the solution mixture within this period. The crude product was collected by filtration. It was dissolved in acetonitrile. Slow evaporation of acetonitrile solution of the compound yielded crystalline [**3**]$(ClO_4)_2$. Yield: 70%. $\Lambda_M = 240\ \Omega^{-1}\ cm^2\ mol^{-1}$ (1×10^{-3} M in acetonitrile). Anal. Calcd for $C_{32}H_{28}N_{10}Cl_2O_{10}Pd_2$: C, 38.54; H, 2.81; N, 14.05. Found: C, 38.58; H, 2.86; N, 14.01.

$[PdCl(L^{1a})]$, 4a. The ligand HL^{1a} (0.1 g, 0.36 mmol) was dissolved in methanol (30 mL), and to it were added 1−2 drops of dilute triethylamine. To the deprotonated ligand solution was added a methanolic solution of $Na_2[PdCl_4]$ (0.11 g, 0.37 mmol), and the mixture was stirred for 30 min at room temperature. The color of the solution changed from orange yellow to brown. The compound was precipitated from the solution mixture within this period. The crude product was collected by filtration and dissolved in dichloromethane. Crystalline **4a** was obtained by slow diffusion of a dichloromehane solution of the compound into hexane. Yield: 80%. Anal. Calcd for $C_{17}H_{13}N_4ClPd$: C, 49.14; H, 3.13; N, 13.49. Found: C, 49.20; H, 3.20; N, 13.42.

The complex **$[PdCl(L^{1b})]$**, **4b**, was synthesized similarly using HL^{1b} in place of HL^{1a}. Yield: 75%. Calcd for $C_{18}H_{15}N_4ClPd$: C, 50.35; H, 3.50; N, 13.05. Found: C, 50.38; H, 3.47; N, 13.08.

$[PtCl_3(L^2)]$, 5. The ligand HL^2 (0.1 g, 0.36 mmol) was dissolved in acetonitrile (30 mL), and to it were added 1−2 drops of dilute triethylamine. To the deprotonated ligand solution was added a solution of $K_2[PtCl_4]$ (0.15 g, 0.36 mmol) in acetonitrile (15 mL), and the mixture was refluxed for 2 h on a steam bath. The color of the solution changed to green. The resultant mixture was filtered and concentrated to 15 mL, from which crystalline green **5** was obtained in 60% yield. Anal. Calcd for $C_{16}H_{12}N_5Cl_3Pt$:C, 33.35; H, 2.08; N, 12.15. Found: C, 33.40; H, 2.02; N, 12.20.

$[PtCl_3(L^{1a})]$, 6a. The ligand HL^{1a} (0.1 g, 0.36 mmol) was dissolved in acetonitrile (30 mL), and to it were added 1−2 drops of dilute triethylamine. To the deprotonated ligand solution was added a solution of $K_2[PtCl_4]$ (0.15 g, 0.36 mmol) in acetonitrile (15 mL), and the mixture was refluxed for 2 h on a steam bath. The color of the solution changed to green. The resultant mixture was filtered and concentrated to 15 mL, from which crystalline green **6a** was obtained in 65% yield. Anal. Calcd for $C_{17}H_{13}N_4Cl_3Pt$: C, 35.50; H, 2.26; N, 9.75. Found: C, 35.55; H, 2.28; N, 9.72.

Similarly the complex **$[PtCl_3(L^{1b})]$**, **6b**, was prepared following the above procedure using HL^{1b} in place of HL^{1a}. Yield: 60%. Anal. Calcd for $C_{18}H_{15}N_4Cl_3Pt$: C, 36.70; H, 2.54; N, 9.51. Found: C, 36.75; H, 2.50; N, 9.55.

X-ray Structure Determination. Crystallographic data for the compounds $[H_2L^2](ClO_4)$, [**2**]$\cdot H_2O$, [**3**]$(ClO_4)_2 \cdot H_2O$, **4a**, and **5** are collected in Table 3.

$[H_2L^2](ClO_4)$. X-ray quality crystals ($0.41 \times 0.09 \times 0.08$ mm^3) of $[H_2L^2](ClO_4)$ were obtained by slow diffusion of an acetonitrile solution of the compound into toluene. The data were collected ($1.97° < \theta < 26.43°$) at 293(2) K on a Bruker SMART CCD 1000 diffractometer equipped with graphite-monochromated Mo Kα radiation ($\lambda = 0.71073$ Å). A total of 10588 reflections were collected, of which 3493 were unique ($R_{int} = 0.0269$). The structure was solved by direct methods using the Program SHELXS-97[22a] and refined by full-matrix least-squares techniques against F^2 using SHELXL-97.[23] Positional and anisotropic atomic displacement parameters were refined for all non-hydrogen atoms.

$[Ni_2Cl_2(L^2)_2] \cdot H_2O$, $2 \cdot H_2O$. X-ray quality crystals ($0.50 \times 0.10 \times 0.08$ mm^3) of $2 \cdot H_2O$ were obtained by slow diffusion of a dichloromethane solution of the compound into hexane. Data were collected ($2.99° < \theta < 24.99°$) at 293(2) K on a Stoe imaging plate diffraction system (IPDS) using Mo Kα radiation

(22) (a) Sheldrick, G. M. *Acta Crystallogr*. **1990**, *46A*, 467. (b) Sheldrick, G. M. *SHELXS-97, Program for the Solution of Crystal Structures*; University of Göttingen: Göttingen, Germany, 1997.
(23) Sheldrick, G. M. *SHELXL-97, Program for the Refinement of Crystal Structures*; University of Göttingen: Göttingen, Germany, 1997.

Table 3. Crystallographic Data

	$[H_2L^2](ClO_4)$	$\mathbf{2}\cdot H_2O$	$[\mathbf{3}](ClO_4)_2\cdot H_2O$[a]	**4a**	**5**
empirical formula	$C_{16}H_{14}N_5ClO_4$	$C_{32}H_{26}N_{10}Cl_2ONi_2$	$C_{32}H_{26}N_{10}Cl_2O_9Pd_2$	$C_{17}H_{13}N_4ClPd$	$C_{16}H_{12}N_5Cl_3Pt$
molecular mass	375.77	754.95	978.33	415.16	575.75
temp (K)	293(2)	293(2)	293(2)	293(2)	150(2)
cryst syst	monoclinic	monoclinic	monoclinic	monoclinic	monoclinic
space group	$P2_1/c$ (No. 14)	$P2_1/n$ (No. 14)	$P2_1/n$	$P2_1/n$	$P2_1/n$
a (Å)	7.3393(19)	16.3100(18)	12.5546(9)	6.7919(5)	11.641(3)
b (Å)	18.897(5)	11.6605(6)	14.4884(11)	16.9123(13)	8.486(2)
c (Å)	12.505(3)	16.9164(12)	21.2438(15)	13.8290(10)	18.402(5)
α (deg)	90	90	90	90	90
β (deg)	98.172(5)	97.387(11)	102.919(2)	91.161(2)	105.817(4)
γ (deg)	90	90	90	90	90
V (Å^3)	1716.7(8)	3190.5(4)	3766.3(5)	1588.2(2)	1749.0(7)
Z	4	4	4	4	4
D_{calcd} (Mg/m^3)	1.454	1.572	1.750	1.736	1.750
cryst dimens (mm^3)	0.41 × 0.09 × 0.08	0.50 × 0.10 × 0.08	0.40 × 0.13 × 0.10	0.40 × 0.15 × 0.11	0.40 × 0.13 × 0.10
θ range for data collection (deg)	1.97−26.43	2.99−24.99	1.73−27.56	1.90−27.49	1.82 −27.50
GOF	1.026	1.064	1.013	0.960	1.008
wavelengths (Å)	0.71073	0.71073	0.71073	0.71073	0.71073
reflns collected	10588	26943	23768	9991	8411
unique reflns	3493	5470	8654	3621	3920
largest diff between peak and hole (e Å^{-3})	0.664, −0.411	0.515, −0.265	0.899, −0.427	0.793, −0.417	1.417, −1.740
final R indices ($I > 2\sigma(I)$)	R1 = 0.0562 wR2 = 0.1434	R1 = 0.0408 wR2 = 0.0719	R1 = 0.0502 wR2 = 0.1073	R1 = 0.0292 wR2 = 0.0536	R1 = 0.0254 wR2 = 0.0510

[a] There are two water molecules with 0.5 occupancy on each oxygen atom.

(λ = 0.71073 Å). A total of 26943 reflections were collected, of which 5470 were unique (R_{int} = 0.0811). The structure was solved by direct methods using the program SHELXS-97[22b] and refined by full-matrix least-squares techniques against F^2 using SHELXL-97.[23] Positional and anisotropic atomic displacement parameters were refined for all non-hydrogen atoms.

$[Pd_2(L^2)_2](ClO_4)_2\cdot H_2O$, $[\mathbf{3}](ClO_4)_2\cdot H_2O$. X-ray quality crystals (0.40 × 0.13 × 0.10 mm^3) of $[\mathbf{3}](ClO_4)_2\cdot H_2O$ were obtained by slow evaporation of an acetonitrile solution of the compound. The data were collected (1.73° < θ < 27.56°) at 293(2) K on a Bruker SMART diffractometer equipped with graphite-monochromated Mo Kα radiation (λ = 0.71073 Å). Data were corrected for Lorentz−polarization effects. A total of 23768 reflections were collected, of which 8654 were unique (R_{int} = 0.0481). The structure was solved by employing the SHELXS-97[22a] program package and refined by full-matrix least squares based on F^2 (SHELXL-97).[23]

$[PdCl(L^{1a})]$, 4a. X-ray quality crystals (0.40 × 0.15 × 0.11 mm^3) of **4a** were obtained by slow diffusion of a dichlomethane solution of the compound into hexane. The data were collected (1.90° < θ < 27.49°) at 293(2) K on a Bruker SMART diffractometer equipped with graphite-monochromated Mo Kα radiation (λ = 0.71073 Å). Data were corrected for Lorentz−polarization effects. A total of 9991 reflections were collected, of which 3621 were unique (R_{int} = 0.0294). The structure was solved by employing the SHELXS-97[22a] program package and refined by full-matrix least squares based on F^2 (SHELXL-97).[23]

$[PtCl_3(L^2)]$, 5. X-ray quality crystals (0.40 × 0.13 × 0.10 mm^3) of **5** were obtained by slow evaporation of a concentrated acetonitrile solution of the compound. The data were collected (1.82° < θ < 27.50°) at 150(2) K on a Bruker SMART diffractometer equipped with graphite-monochromated Mo Kα radiation (λ = 0.71073 Å). Data were corrected for Lorentz−polarization effects. A total of 8411 reflections were collected, of which 3920 were unique (R_{int} = 0.0370). The structure was solved by employing the SHELXS-97[22a] program package and refined by full-matrix least squares based on F^2 (SHELXL-97).[23]

Acknowledgment. Financial support received from the Department of Science and Technology, New Delhi, is gratefully acknowledged. The magnetic work carried out at ICMA was supported by Grant MAT02/166 from CICYT, and M.D.K. acknowledges receiving a fellowship from Ministerio de Educación, Culturay Deporte of Spain, No. SAB2000-0084.

Supporting Information Available: ^{1}H NMR spectrum of the complex $[\mathbf{1}](ClO_4)$ in $CDCl_3$, a plot of magnetic moment vs magnetic field, results of low-temperature magnetization, and X-ray crystallographic details in CIF format of the five compounds $[H_2L^2](ClO_4)$, $\mathbf{2}\cdot H_2O$, $[\mathbf{3}](ClO_4)_2\cdot H_2O$, **4a**, and **5**. This material is available free of charge via the Internet at http://pubs.acs.org.

IC034313H